[11C]deschloroclozapine is an improved PET radioligand for quantifying a human muscarinic DREADD expressed in monkey brain

Xuefeng Yan[1], Sanjay Telu[1], Rachel M Dick[1] , Jeih-San Liow[1],
Paolo Zanotti-Fregonara[1], Cheryl L Morse[1], Lester S Manly[1],
Robert L Gladding[1], Stal Shrestha[1], Walter Lerchner[2],
Yuji Nagai[3], Takafumi Minamimoto[3] , Sami S Zoghbi[1],
Robert B Innis[1], Victor W Pike[1], Barry J Richmond[2] and
Mark AG Eldridge[2]

Abstract

Previous work found that [11C]deschloroclozapine ([11C]DCZ) is superior to [11C]clozapine ([11C]CLZ) for imaging Designer Receptors Exclusively Activated by Designer Drugs (DREADDs). This study used PET to quantitatively and separately measure the signal from transfected receptors, endogenous receptors/targets, and non-displaceable binding in other brain regions to better understand this superiority. A genetically-modified muscarinic type-4 human receptor (hM$_4$Di) was injected into the right amygdala of a male rhesus macaque. [11C]DCZ and [11C]CLZ PET scans were conducted 2–24 months later. Uptake was quantified relative to the concentration of parent radioligand in arterial plasma at baseline (n = 3 scans/radioligand) and after receptor blockade (n = 3 scans/radioligand). Both radioligands had greater uptake in the transfected region and displaceable uptake in other brain regions. Displaceable uptake was not uniformly distributed, perhaps representing off-target binding to endogenous receptor(s). After correction, [11C]DCZ signal was 19% of that for [11C]CLZ, and background uptake was 10% of that for [11C]CLZ. Despite stronger [11C]CLZ binding, the signal-to-background ratio for [11C]DCZ was almost two-fold greater than for [11C]CLZ. Both radioligands had comparable DREADD selectivity. All reference tissue models underestimated signal-to-background ratio in the transfected region by 40%–50% for both radioligands. Thus, the greater signal-to-background ratio of [11C]DCZ was due to its lower background uptake.

Keywords

Introduction

Designer Receptors Exclusively Activated by Designer Drugs (DREADDs) are a chemogenetic technology used to manipulate neuronal activity in vivo.[1,2] In most experimental designs, a genetically modified receptor is virally transfected into a neuronal population in a selected brain region. The transfected receptor can be activated by a systemically administered designer drug, which is intended to act only at the transfected

[1]Molecular Imaging Branch, National Institute of Mental Health, National Institutes of Health, Bethesda, MD, USA
[2]Laboratory of Neuropsychology, National Institute of Mental Health, National Institutes of Health, Bethesda, MD, USA
[3]Department of Functional Brain Imaging, National institute of Radiological Sciences, National Institutes for Quantum and Radiological Science and Technology, Chiba, Japan

Corresponding author:
Xuefeng Yan, Molecular Imaging Branch, National Institute of Mental Health, 10 Center Drive, Bldg. 10, Rm B1D43, Bethesda, MD 20892, USA.
Email: xuefeng.yan@nih.gov

receptor and not at endogenous receptors. Depending on the type of transfected receptor, its activation may cause electrical excitation or inhibition of the neuronal population.[3–6] Using the radiolabeled version of the designer drug, positron emission tomography (PET) imaging can be used to quantify the in vivo density and distribution of the transfected receptor.[7–10] Such PET studies are important for establishing whether the transfection was successful and what region(s) were affected.

The prototypical agonist for the muscarinic DREADDs, clozapine-*N*-oxide (CNO), has been used to both pharmacologically activate the transfected receptor and, when radiolabeled as [^{11}C]CNO, to localize and quantify the transfected receptor in rodents using PET.[8] Because it is a substrate for efflux transporters such as P-glycoprotein at the blood-brain barrier, only limited amounts of CNO accumulate in the brain. In rhesus monkeys, the brain penetrance of [^{11}C] CNO is so low that it is not a viable PET ligand.[7] However, CNO is rapidly converted in the periphery to clozapine (CLZ), which readily enters the brain.[11–13] Thus, both the pharmacological and radiolabeling properties of CNO are thought to derive from CLZ rather than CNO.[11]

Nagai and colleagues recently developed deschloro-clozapine (DCZ), which is superior to CNO as both a pharmacological activator and as a PET radioligand.[7] Their study demonstrated that the signal-to-background ratio of [^{11}C]DCZ was higher than that of [^{11}C]CLZ, observable as higher contrast of the hot spot of transfection compared to non-transfected control region or to the rest of the brain. For this comparison, the signal-to-background ratio was measured via relative tracer uptake, suggesting that [^{11}C]DCZ has higher target-selective binding and/or lower nonspecific binding than [^{11}C]CLZ.

On the basis of in vitro binding studies, Nagai and colleagues further demonstrated that [^{11}C]DCZ has less off-target binding than [^{11}C]CLZ to numerous endogenous receptors, suggesting that the superior contrast image might be partly due to reducing noise from off-target binding. However, the extent of the reduced off-target binding of [^{11}C]DCZ remains unclear because the in vivo binding of a radioligand is the product of the affinity of the radioligand and the density of the receptor.[14] In addition to specific binding, the PET signal reflects localization of radioligand in the other compartment (i.e., non-specific binding), producing noise as background signal. Indeed, clozapine and its analogs have been shown to display non-specific brain tissue binding.[7,15]

This study was undertaken to assess why [^{11}C]DCZ has superior imaging properties to [^{11}C]CLZ, which is the active radiometabolite of [^{11}C]CNO.

Two properties of interest were investigated: signal-to-background ratio and selectivity for the transfected receptor. Quantitative imaging was performed in monkey brain using [^{11}C]DCZ and [^{11}C]CLZ. Although the previous study by Nagai and colleagues measured uptake as a ratio of radioactivity in various brain regions—e.g., the ratio of transfected region to non-transfected region[7]—such a ratio cannot distinguish between high affinity (i.e., displaceable) binding of the radioligand to the transfected receptor and to endogenous receptor(s) versus low affinity (i.e., non-displaceable) binding to unknown targets. By quantifying brain uptake relative to the parent radioligand in arterial plasma, the present study measured the components of radioligand binding to target and non-target as well as other background, appropriately weighted by the affinity of each radioligand and the density of each target.

Materials and methods

A note on terminology

"Signal-to-background ratio", as used herein, might also be called "signal-to-noise ratio". Although no consensus exists, "noise" in medical physics often refers to measurement errors – i.e., something that does not actually exist in the tissue. In this context, noise is a component of measurement for all signals, including on-target binding, off-target binding, and nondisplaceable uptake; it does not refer to an unintended target of a radiotracer. Given that "noise" can be confusing, we chose to use the clearer "signal-to-background ratio", with signal defined as what we intend to measure (i.e., binding to the transfected receptor $V_{\text{S-on}}$). In addition, BP_{ND} is used according to its consensus definition, that is, the ratio of specific binding to non-displaceable uptake (V_{ND}). Thus, "signal-to-background ratio" is fully defined as a slightly modified $BP_{\text{ND}}' = V_{\text{S-on}}/V_{\text{ND}}$. Please note that both BP_{ND} and BP_{ND}' reflect contrast in the image, and we reserved the term "contrast" to refer to a visual characteristic of the PET images.

Radiochemistry and chemicals

Reference CLZ, desmethyl-CLZ (Sigma-Aldrich, St. Louis, MO), a precursor for [^{11}C]CLZ synthesis, reference DCZ (MedChemExpress LLC, Monmouth Junction, NJ), and DREADD agonist 21 (Tocris, Minneapolis, MN), a precursor for [^{11}C]DCZ synthesis, were obtained from commercial sources. Anhydrous acetonitrile (Sure-seal) was purchased from VWR (Radnor, PA). To protect personnel from radiation, radiochemistry was performed in a

lead-shielded hot-cell with an automated radiosynthesis apparatus, a modified Synthia platform controlled with software based on Labview and developed in-house.[16,17]

No-carrier-added [11C]carbon dioxide ($\sim$ 60 GBq) was produced with the $^{14}N(p,\alpha)^{11}C$ nuclear reaction by bombarding a nitrogen–1% oxygen gas target (initial pressure 300 psi) for 20 minutes with a proton beam (16.5 MeV, 45 μA) obtained from a biomedical cyclotron (PETtrace, GE Medical Systems: Severna Park, MD). No-carrier-added [11C]iodomethane was produced from [11C]carbon dioxide in a PETtrace MeI Process Module. In this apparatus, the [11C]carbon dioxide was reduced to [11C]methane, which was then iodinated via recirculation over heated iodine crystals at 720 °C.[18] [11C]Methyl triflate was then produced by passing the [11C]iodomethane over heated (220 °C) silver triflate.[19]

Radiosynthesis of [11C]CLZ

[11C]Methyl triflate was trapped in a crimp-sealed 1-mL high recovery vial containing desmethyl-CLZ (1.0 ± 0.1 mg, 3.2 μmol) in acetonitrile (0.3 mL) and heated at 50 °C for five minutes. These and subsequent data are expressed as mean±SD. The reaction mixture was quenched with water (3 mL), and [11C]CLZ was isolated with a reversed-phase high-performance liquid chromatography (HPLC) system (Beckman Coulter; Fullerton, CA) using a Luna C18(2) column (10 × 250 mm, 5 μm; Phenomenex; Torrance, CA) eluted with MeCN − 100 mM aq MeCOONH$_4$ (50:50 v/v) at 4 mL/min (retention time (t_R) = 13.5 min). After removal of the mobile phase (rotary evaporation for one minute), [11C]CLZ was formulated for intravenous injection in sterile ethanol-saline (10:90 v/v; 10 mL) and sterile-filtered (Millex-MP 0.22 μm, 25 mm). The identity of [11C]CLZ was confirmed with reversed-phase HPLC analysis on a LiChrospher RP-18e column (4.0 mm × 125 mm, 5 μm; Phenomenex) eluted with MeCN − 100 mM aq MeCOONH$_4$ (50:50 v/v) at 1 mL/min (t_R = 5.7 min), and with liquid chromatography-mass spectrometry (LC-MS) of associated carrier: (m/z) $[M + H]^+$: 327.1. The synthesis process lasted 50 ± 2 minutes. This radiotracer product was radiochemically stable over its period of use.

Radiosynthesis of [11C]DCZ

[11C]Methyl triflate was trapped in a crimp-sealed 1-mL high recovery vial containing precursor desmethyl-DCZ (0.5 ± 0.1 mg, 1.8 μmol) in acetonitrile (0.3 mL) and heated at 50 °C for five minutes. The reaction mixture was quenched with water (3 mL), and [11C]DCZ was isolated with a reversed-phase HPLC

system (KNAUER; Germany) using an X-Bridge BEH C18 OBD column (10 × 250 mm, 10 μm; Waters; Milford, MA) eluted with MeCN−water-Et$_3$N (40:60:0.1 by vol., pH 10) at 5 mL/min (t_R = 10.2 min). After removal of the mobile phase (rotary evaporation for one minute), [11C]DCZ was formulated for intravenous injection in sterile ethanol-saline (10:90 v/v; 10 mL) and sterile-filtered (Millex-MP 0.22 μm, 25 mm). The identity of [11C]DCZ was confirmed with reversed phase HPLC analysis on a CAPCELL PAK C18 UG120 S5 (4.6 mm × 150 mm, 5 μm; Phenomenex, Torrance, CA) eluted with MeCN−water-Et$_3$N (40:60:0.1 by vol., pH 10) at 1 mL/min (t_R = 7.5 min) and with LC-MS of associated carrier: (m/z) $[M + H]^+$: 293.2. The synthesis process lasted 42 ± 2 minutes. This radiotracer product was radiochemically stable over its period of use.

Transfection of DREADDs in monkey brain

All studies were conducted in accordance with "Animal Research: Reporting of In Vivo Experiments" guidelines as well as Guidelines for the Care and Use of Laboratory Animals, 8th Edition, and were approved by the National Institute of Mental Health Animal Care and Use Committee. A lentivirus carrying an hM$_4$Di-CFP fusion protein expressed under a human synapsin promoter (Lenti-hSyn-hM$_4$Di, 10^9 infectious particles/mL) was injected into the right amygdala of a single rhesus macaque (11-year-old male). Twenty μL of virus was injected at each of 10 locations spaced approximately 2 mm apart in the medio-lateral, dorso-lateral, and/or antero-posterior planes. The surgery was performed under aseptic conditions in a fully equipped operating suite.

Magnetic resonance imaging

A magnetic resonance imaging (MRI) scan was performed after brain injection using a 3 T MRI scanner (Achieva dStream, Philips Healthcare, Best, Netherlands), as previously described.[20] For all MRI procedures, anesthesia was performed with ketamine (10 mg/kg, i.m.) and dexmedetomidine (0.2 mL, i.m.).

PET scanning and image processing

For each radioligand, six scans (three baseline and three blocked) were performed in a single monkey using a microPET Focus 220 scanner (Siemens Medical Solutions; Knoxville, TN). Baseline scans were performed in the morning and blocked scans were performed in the afternoon of the same day. The interval between imaging sessions was at least three weeks. The weight of the animal varied little during the total period of the studies (body

weight = 11.6 ± 0.9 kg). The blocking agent was intravenously administered 10–20 minutes before the radioligand. For [^{11}C]CLZ, the three blocking agents were: a) CNO (10 mg/kg), b) CLZ (0.1 mg/kg), and c) clotrimazole (CTM; 1 mg/kg, a metabolic inhibitor of CNO[21]) plus CNO (10 mg/kg). For [^{11}C]DCZ, the three blocking agents were: a) CNO (10 mg/kg), b) low-dose DCZ (0.1 mg/kg), and c) high-dose DCZ (1 mg/kg). PET images were acquired after injection of [^{11}C]CLZ (278 ± 64 MBq) or [^{11}C]DCZ (302 ± 51 MBq) for two hours, with frame duration ranging from 30 seconds to 10 minutes. For all PET imaging procedures, anesthesia was induced with ketamine (10 mg/kg, i.m.) and then maintained with 1–2% isoflurane and 98% O_2. Electrocardiogram, body temperature, heart rate, blood pressure, pulse oximetry, and respiratory rate were monitored throughout the scans.

PET imaging data were reconstructed using Fourier rebinning plus two-dimensional filtered backprojection with attenuation and scatter correction. Images were co-registered to a standardized monkey MRI template using PMOD software (PMOD Technologies, LLC, Zurich, Switzerland). Thirty-five predefined brain regions of interest from the template were applied to the co-registered PET image to obtain regional time-activity curves. The target (DREADD) region was drawn manually based on post-operative MRI. Brain uptake was expressed as standardized uptake value (SUV), which normalizes for injected radioactivity and body weight.

Blood input function and radiometabolite analysis

Arterial blood sampling was performed in all scans for radiometabolite analysis to determine radioligand plasma concentrations. About 15 blood samples were drawn from an arterial port in the femoral artery during the 120-minute PET scans. Samples were drawn every 15 seconds for the first two minutes and then at 3, 5, 10, 30, 60, 90, and 120 minutes (varying from 1.0 to 3.0 mL). The parent radioligand concentration and free fraction in plasma (f_P) were measured as previously described.[22]

Modeling methods and time-stability analysis

To assess the radiotracers' transfer between plasma and brain quantitatively, eight different volume-of-interest (VOI)-based methods were performed. The one- and two-tissue compartment models used arterial blood sampling for blood input correction. Total distribution volume (V_T) was calculated accordingly. Total blood volume (Vb) was a fixed value of 5%, because V_T values obtained with a fixed or estimated Vb were comparable. The remaining six methods were based on the

reference tissue model: Ichise's multilinear reference tissue models (MRTM, MRTM0, and MRTM2), simplified reference models (SRTM and SRTM2), and Logan's reference tissue model (Logan-REF). Parameters were corrected for f_P to reflect radioligand binding in the brain that is independent of varying amounts of binding to plasma proteins. The Lassen plot was applied to calculate receptor occupancy and non-displaceable distribution volume (V_{ND}). To determine the minimum scan duration needed to reliably measure V_T, as well as to indirectly assess whether radiometabolites accumulate in the brain, the time stability of V_T was examined by increasingly truncating the scan duration from 120 minutes down to 30 minutes in 10-minute increments. For visualization, parametric images were generated using Ichise's multilinear analysis (MA1) because it minimizes the bias induced by noise in the measurements.[23]

Model comparison and correlation analysis

The optimal plasma input model (i.e. one- vs. two-tissue compartment models) was chosen based on the Akaike information criterion,[24] the model selection criterion,[25] and F-tests. The most appropriate model had the smallest Akaike information criterion and the largest model selection criterion value. F-statistics were used to compare goodness-of-fit for the one- and two-tissue compartment models. A value of p < 0.05 was considered significant. Pearson correlation for binding potential (BP_{ND}) was performed to estimate the correlation of these modeling methods. The Bland-Altman plot was used to assess the bias between models by calculating the means and percentage differences.

Ex vivo rat studies

Rats were anesthetized with 1.5% isoflurane in oxygen. [^{11}C]CLZ and [^{11}C]DCZ (350 µL; 55 MBq) were then injected intravenously through the penile vein of each rat. Thirty minutes after injection of each radioligand, a large anticoagulated (heparin) blood sample was drawn from each rat. The rats were then immediately euthanized by decapitation, and their brains were excised.

Plasma. After separation from blood cells, plasma samples (450 µL) were deproteinated with acetonitrile (720 µL) and samples of 50 µL each were then quantified for radioactivity, as previously described,[26] in an automatic gamma counter (model 1480 Wizard; Perkin-Elmer) with an electronic window set at 360–1800 keV (counting efficiency = 51.84%).

Brain. The radioactivity of brain tissue was also counted in the gamma counter before homogenization in 1.5–3.0 mL of CH_3CN using a handheld tissue Tearor (model 985-370; BioSpec Products Inc. Racine, WI) as well as after homogenization following the addition of 0.5–1.0 mL H_2O. These homogenates were counted in the gamma counter to calculate the percentage recovery of radioactivity into the acetonitrile extracts. Decay corrections of all tissue assays were performed for physical decay with a half-life of 20.4 minutes.[27] The homogenates were then centrifuged at 10,000 g for one minute. The clear supernates were injected onto the HPLC column through nylon filters. Radioactivity in the resulting precipitates was used to calculate the percent recovery of activity in the CH_3CN supernates.

Radio-HPLC was performed on an X-terra® C_{18} column (10 μm, 7.8 mm x 300 mm, Waters Corp., Milford, MA) eluted with methanol: water: triethylamine (80:20:0.1; by volume) at a flow rate of 4.0 mL/min for [11C]CLZ; the condition for [11C]DCZ was with methanol: water: triethylamine (82.5:17.5:0.1; by volume) at a flow rate of 5.0 mL/min. Eluates were monitored with an in-line flow-through NaI (Tl) scintillation detector (Bioscan). Data were stored and analyzed using "Bio-ChromeLite" software. The collection of data for each radiochromatogram was decay corrected according to its respective HPLC injection time.

Results

Radiochemistry

[11C]CLZ and [11C]DCZ were labeled using [11C]methyl triflate produced from cyclotron-produced [11C]carbon dioxide and were obtained with high radiochemical purity (>99%) and high molar activity (Supplementary Figure S1). [11C]CLZ was obtained with $12.3 \pm 4.8\%$ yield and a molar activity of 278 ± 164 GBq/μmol (n = 41). [11C]DCZ was obtained with $18.8 \pm 2.2\%$ yield and a molar activity of 361 ± 130 GBq/μmol (n = 18).

Pharmacological effects

No detectable changes in body temperature, blood pressure, pulse, respiratory rate, EKG, or pulse oximetry were observed after injection of either [11C]CLZ (140 ± 70 pmol/kg) or [11C]DCZ (100 ± 10 pmol/kg).

Plasma analysis

The time-activity curves of parent radioligand in arterial plasma were similar for both [11C]CLZ and [11C]DCZ (Figure 1). As expected from an injection over 120 seconds, concentrations peaked within one to two minutes followed by a rapid decline caused by distribution to organs of the body and then a slower elimination phase. The baseline plasma time-activity curves were minimally affected by pre-injection of blocking drugs: CNO, CLZ, DCZ, or CNO plus CTM. The f_P value of [11C]DCZ ($22 \pm 2\%$, n = 18) was almost four-fold higher than that of [11C]CLZ ($6 \pm 1\%$, n = 18). After V_T/f_P correction, there might be about 16-fold induced variation for [11C]CLZ, and 4-fold for [11C]DCZ.

The radiochromatograms (Supplementary Figure S2A and S2C) of plasma acquired at 30 minutes post-injection showed that radiometabolites, eluting before the parent tracer, constituted most of the radioactivity: 41% for [11C]CLZ and 38% for [11C]DCZ. The percentage composition over time (Supplementary Figure S2B and S2D) for both radioligands was also similar, as 50% composition occurred slightly before 30 minutes for both.

### Kinetic analysis of brain uptake

After [11C]CLZ or [11C]DCZ injection, all brain PET images showed high concentrations of radioactivity followed by moderate washout in all regions. For [11C]CLZ, radioactivity accumulated in the target region (hM4Di) and plateaued as high as 6 ± 1 SUV in the late phase of baseline scans; furthermore, the radioactivity accumulation was displaceable after a rapid peak in blocked scans (Figure 2(a)). [11C]DCZ had similar time-activity curves to [11C]CLZ with a slightly higher radioactivity accumulation at 7 ± 1 SUV in baseline scans (Figure 2(c)). Time-activity curves showed no significant differences between baseline and blocked scans, except for the cerebellum after CNO blockade (Figure 2(b) and (d)). In this case, the higher uptake was presumably caused by higher blood flow to the cerebellum compared to other regions. It should be noted that compartmental modeling corrects for such regional differences in blood flow, assuming that blood flow remains the same for each region during the course of the scan.

Three major findings emerged from kinetic analysis of brain and plasma data for [11C]CLZ and [11C]DCZ: (1) regional brain data were better fit to a two-tissue compartment model than to a one-tissue compartment model; (2) displaceable off-target binding was observed in all brain regions; and (3) lower non-displaceable uptake of [11C]DCZ compared to [11C]CLZ was responsible for its higher signal-to-background ratio.

As regards the first finding, unconstrained two-tissue compartmental fitting converged in all regions and in all scans for both [11C]CLZ and [11C]DCZ. F-test results indicated that the two-tissue compartment model was superior to the one-tissue compartment
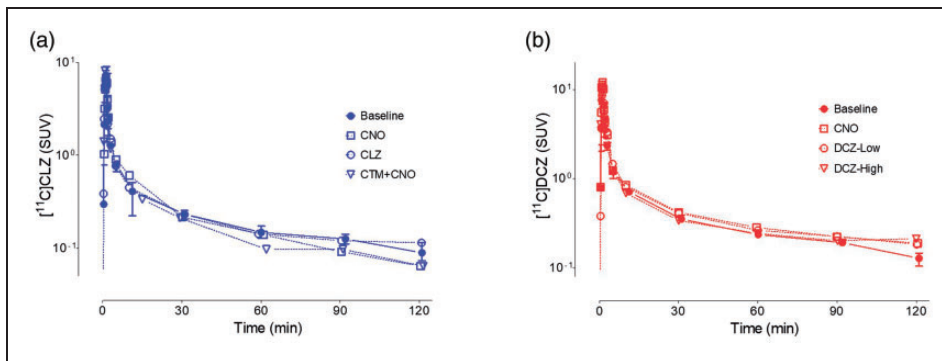
Figure 1. Concentration of (a) [¹¹C]clozapine ([¹¹C]CLZ) and (b) [¹¹C]deschloroclozapine ([¹¹C]DCZ) in arterial plasma at baseline (n = 3 scans per radioligand) and after blockade by CLZ and its analogs, administered 10 minutes before the radioligands. The baseline scans for each radioligand were performed three times. The solid symbols represent means, and the error bars extend to the highest and lowest value among the three measurements. For [¹¹C]CLZ, the three blocking studies and i.v. doses were: (a) clozapine-*N*-oxide (CNO) (10 mg/kg), (b) CLZ (0.1 mg/kg), and (c) clotrimazole (CTM; 1 mg/kg) plus CNO (10 mg/kg). For [¹¹C]DCZ, the three blocking studies and i.v. doses were: (a) CNO (10 mg/kg), (b) low-dose DCZ (0.1 mg/kg), and (c) high-dose DCZ (1 mg/kg).
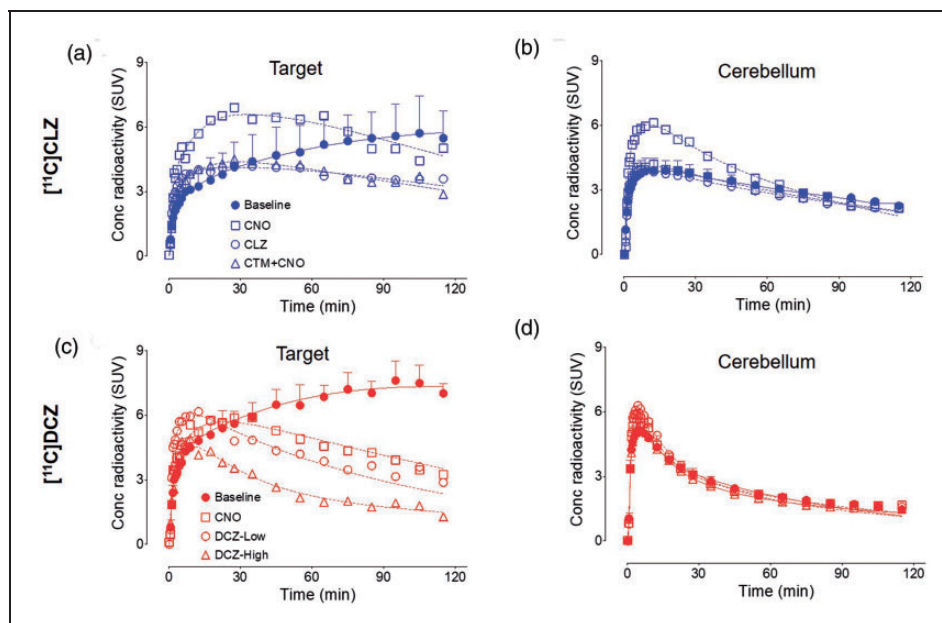
Figure 2. Time-activity curves of the target region and cerebellum for [¹¹C]clozapine ([¹¹C]CLZ) (a and b) and [¹¹C]deschloro-clozapine ([¹¹C]DCZ) (c and d). For the baseline scans (three for each radioligand), the solid symbols represent mean ± SD. The doses of the blocking agents are provided in the legend of Figure 1.

model in all regions for both radioligands ($F_{p(0.05)}$=3.5, $F_{[11C]CLZ}$=17.2 and $F_{[11C]DCZ}$=29.8). In addition, the two-tissue compartment model had a lower mean Akaike information criterion (141 ± 26 for [¹¹C]CLZ and 138 ± 22 for [¹¹C]DCZ) and a higher mean model selection criterion (4.5 ± 0.8 for [¹¹C]CLZ and 4.7 ± 0.9 for [¹¹C]DCZ) than the one-tissue compartment model (Akaike information criterion: 153 ± 29 and 154 ± 20 for [¹¹C]CLZ and [¹¹C]DCZ, respectively; model selection criterion: 4.0 ± 0.8 and 3.9 ± 0.8 for [¹¹C]CLZ and [¹¹C]DCZ, respectively, p < 0.01).

As regards the second finding, both radioligands had widespread displaceable binding in all brain regions (Figure 3 and Supplementary Table S1). That is, CLZ and DCZ showed considerable displaceable (also called high affinity or specific) binding to the transfected receptor (i.e., on-target) and to endogenous receptor(s) (i.e., off-target). For this reason, specific distribution volume (V_S) was separated into its two components: V_{S-on} (i.e., bound to the transfected receptor) and V_{S-off} (i.e., bound to endogenous receptors). Thus, the compartmental model used to analyze these
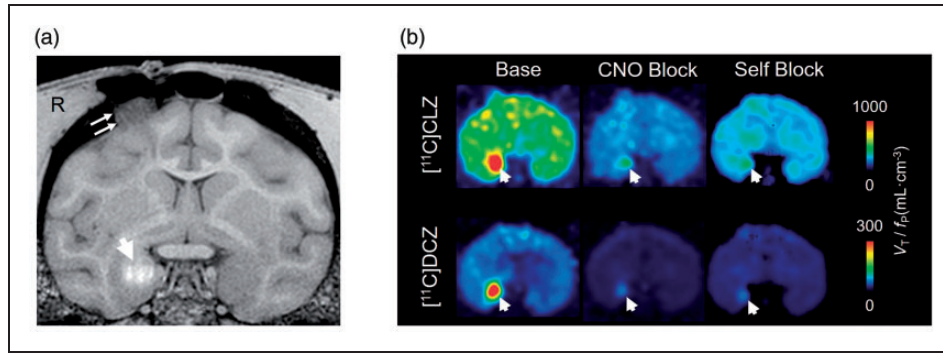
Figure 3. Magnetic resonance imaging (MRI) (a) and positron emission tomography (PET) (b) images of the monkey with Designer Receptors Exclusively Activated by Designer Drug (DREADD) injected into the right amygdala. The T1-weighted MRI (a) shows the contrast enhancer (Mn^{++}) at the injection site (marked with arrow). PET images (b) display the calculated values of binding corrected for the free fraction in plasma of the radioligand (V_T/f_P). The baseline image of [^{11}C]deschloroclozapine ([^{11}C]DCZ) compared to that of [^{11}C]clozapine ([^{11}C]CLZ) clearly shows greater contrast between the injection site (marked with an arrow) and the surrounding brain. Blockade by clozapine-*N*-oxide (CNO) (10 mg/kg i.v.) and the nonradioactive ligand (self-block 0.1 mg/kg i.v.) were 70–83% complete, based on Lassen analysis.

results included two types of specific/displaceable binding, and the standard nomenclature was correspondingly modified (Supplementary Table S2).[14]

Using this separation into two types of specific binding, a new type of binding potential was defined that equaled the ratio of $V_{S\text{-on}}$ to nondisplaceable distribution volume (V_{ND}): BP_{ND}'. This term is distinct from standard BP_{ND}, which is the ratio of V_S to V_{ND}.

$$V_S = V_{S\text{-on}} + V_{S\text{-off}}$$
$$BP_{ND} = V_S/V_{ND}$$
$$BP_{ND}' = V_{S\text{-on}}/V_{ND}$$

A previous study found that no significant change in [^{11}C]CLZ uptake was induced by injection of control virus.[7] Assuming that the transfected receptor did not spread from the right amygdala to the contralateral region, $V_{S\text{-on}}$ reflects the difference between the right and left amygdalae. Therefore, $V_{S\text{-off}}$ reflects the displaceable binding in all regions except the right amygdala (Supplementary Table S3).

As regards the third finding, [^{11}C]DCZ had lower non-displaceable uptake than [^{11}C]CLZ. As noted in the Methods, three baseline and three blocked studies were performed for each radioligand in order to determine V_{ND}. Because the blockades were incomplete, Lassen plot was used to extrapolate V_{ND} to that associated with 100% occupancy of the transfected and endogenous receptor(s) (Figure 4). Using this approach, the $V_{S\text{-on}}/f_P$ for [^{11}C]DCZ was one-fifth of that for [^{11}C]CLZ, and the V_{ND}/f_P for [^{11}C]DCZ was one-tenth of that for [^{11}C]CLZ (Table 1). The net effect of these two variables was that the BP_{ND}' of [^{11}C]DCZ was 1.8-fold higher than that of [^{11}C]CLZ. The coefficient of variation (COV) for BP_{ND}' was 0.15 for [^{11}C]DCZ, which was two-fold lower than that for [^{11}C]
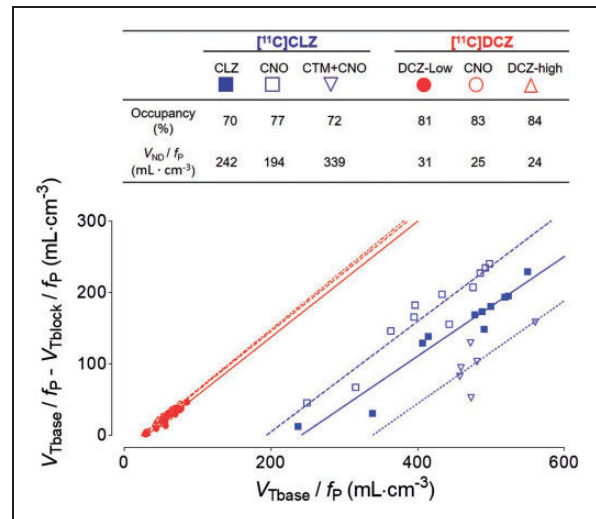
Figure 4. Lassen plot for [^{11}C]clozapine ([^{11}C]CLZ) and [^{11}C]deschloroclozapine ([^{11}C]DCZ), each studied after three blocking drugs (see Figure 1). The slope of each line equals the occupancy induced by the blocking drug, and the *x*-intercept represents nondisplaceable uptake corrected for free fraction in plasma (V_{ND}/f_P). Although not obvious from the graph, the range of the values of the *x*-intercepts show a similar relative dispersion. The mean (mL $\cdot$cm^{-3}) $\pm$ coefficient of variation (COV) (%) of V_{ND}/f_P was $258 \pm 29\%$ for [^{11}C]CLZ and $27 \pm 14\%$ for [^{11}C]DCZ. The target region (shown in Figure 6) was excluded from the regression because of its high and non-linear value.

CLZ. The results of these analyses are displayed in Figure 5 as parametric images of V_S, $V_{S\text{-on}}$, $V_{S\text{-off}}$, and V_{ND}, all corrected for f_P. Both the $V_{S\text{-on}}/f_P$ and V_{ND}/f_P of [^{11}C]DCZ were much lower than those of [^{11}C]CLZ.

Table 1. Brain uptake parameters* of [^{11}C]clozapine ([^{11}C]CLZ) and [^{11}C]deschloroclozapine ([^{11}C]DCZ) in the right amygdala of a rhesus monkey.

Parameter	[^{11}C]CLZ	[^{11}C]DCZ	Percentage (CLZ/DCZ)
$V_{\text{S-on}} / f_P$ (mL·cm^{-3})	990 ± 130	190 ± 38	5.2
$V_{\text{S-off}} / f_P$ (mL·cm^{-3})	192 ± 70	32 ± 7	6.0
V_{ND} / f_P (mL·cm^{-3})	258 ± 74	27 ± 4	9.6
BP_{ND}'	4 ± 1	7 ± 1	0.6
Percentage on-target (%)	84 ± 4	85 ± 4	1.0

DREADD: Designer Receptors Exclusively Activated by Designer Drug; V_{ND}: non-displaceable distribution volume; $V_{\text{S-on}}$: on-target displaceable binding (i.e., to the transfected receptor); $V_{\text{S-off}}$: off-target distribution volume (i.e., to endogenous receptors); BP_{ND}': ratio of target binding to nondisplaceable uptake ($V_{\text{S-on}}/V_{\text{ND}}$) . V_{ND}, $V_{\text{S-off}}$, and $V_{\text{S-on}}$ were corrected for the free fraction in plasma (f_P) of the radioligand. The percentage of off-target binding was calculated as $V_{\text{S-off}}/(V_{\text{S-on}} + V_{\text{S-off}})$.

*All parameters (mean ± standard deviation (SD)) were determined from three baseline and three blocked scans for each radioligand in a rhesus monkey injected with DREADD in the right amygdala.
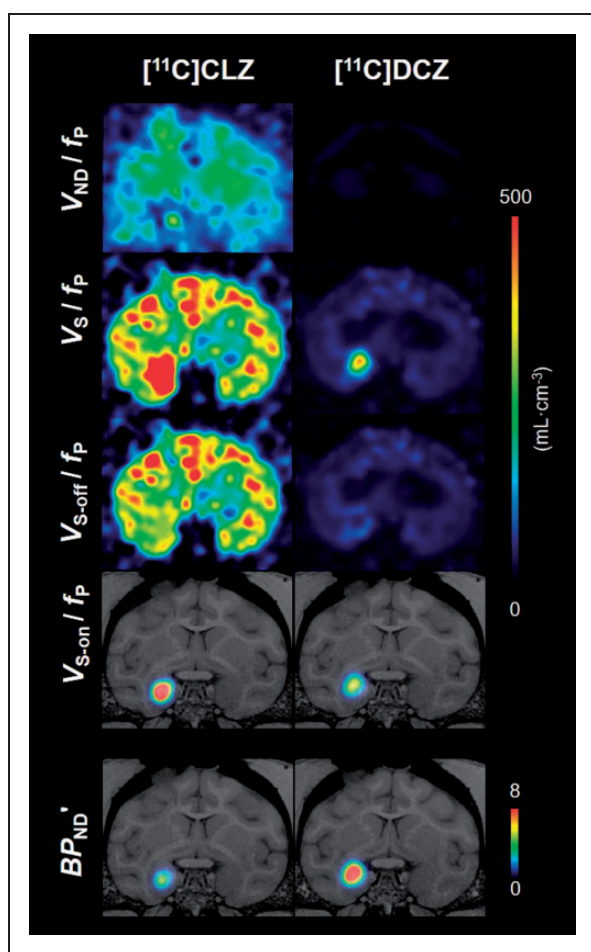
Figure 5. Ichise's multilinear analysis (MA1)-derived parametric images for [^{11}C]clozapine ([^{11}C]CLZ) and [^{11}C]deschlorocloza-pine ([^{11}C]DCZ). Parameters were determined from baseline and blockade scans (clozapine-N-oxide (CNO) 10 mg/kg i.v.). Four distribution volumes are displayed and corrected for free fraction in plasma (f_P): V_{ND}, nondisplaceable distribution volume; V_S, specific distribution volume (i.e., all displaceable binding); $V_{\text{S-off}}$, off-target distribution volume; and $V_{\text{S-on}}$, on-target distribution volume. The modified binding potential BP_{ND}' is the ratio of $V_{\text{S-on}}$ to V_{ND}.

In addition, the selectivity of each radioligand for the transfected receptor was expressed in the percentage of on-target binding to total specific binding: $V_{\text{S-on}}/(V_{\text{S-on}} + V_{\text{S-off}})$. Both radioligands had similar selectivity: 84% for [^{11}C]CLZ and 85% for [^{11}C]DCZ.

Finally, V_T values for both [^{11}C]CLZ and [^{11}C]DCZ were stable within 90 minutes of imaging (Supplementary Figure S3). That is, V_T values were within 10% of that at 120 minutes. This time stability suggests that radiometabolites were not accumulating in the brain.

Reference tissue models

If a reference region devoid of receptors exists in the brain, that region can substitute for the plasma input function and avoid the need for repeated arterial blood samples. To assess the accuracy of reference tissue models, we compared the "gold standard" analysis using compartmental modeling and serial concentrations of the parent radioligand in arterial plasma (described above) with several reference tissue models: MRTM, MRTM0, MRTM2, SRTM, SRTM2, and Logan-REF. The cerebellum was selected as the reference region, as it was far from the injection site. Although good correlation (r > 0.90) was observed between kinetic methods with or without plasma input (Figure 6(a)), MRTM underestimated BP_{ND} by 43% for [^{11}C]CLZ and 63% for [^{11}C]DCZ in the DREADD-injected region. In all other brain regions, MRTM underestimated BP_{ND} by 28% for [^{11}C]CLZ and 51% for [^{11}C]DCZ (Figure 6(b)). The other five reference tissue methods exhibited similar results to MRTM (data not shown). The bias of reference tissue models was caused by violations in the assumptions of these models, including, but not limited to, the presence in
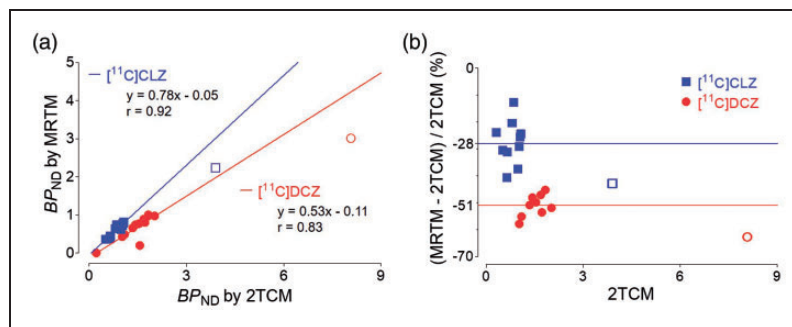
Figure 6. Comparison of a multilinear reference tissue model (MRTM) and the "gold standard" two-tissue compartment model (2TCM) for [11C]clozapine ([11C]CLZ) and [11C]deschloroclozapine ([11C]DCZ). For each radioligand, binding potential (BP_{ND}) was determined from baseline and blocking scans (clozapine-N-oxide (CNO) 10 mg/kg i.v.). The Pearson correlation plots (a) show that BP_{ND} of the two models was well correlated in all regions except the injection site (highest values in upper right). The injection site was not included in the correlation analysis and was underestimated relative to the linear extension of all other regions. The Bland-Altman plots (b) in the non-target regions showed an average underestimation of 28% for [11C]CLZ and 51% for [11C]DCZ. For both radioligands, the underestimation in the transfected region (two right-most symbols) was even greater than in the non-target regions.

cerebellum of some specific (i.e., blockable) uptake of radioligand.[28]

Radiometabolites in rat brain

Compartmental modeling assumes that radioactivity in brain measured via PET derives from parent radioligand and not from radiometabolites. To test this assumption, both [11C]CLZ and [11C]DCZ were injected into rats. Most of the radioactivity extracted from the brain for both radioligands was found to be parent radioligand: 97% for [11C]DCZ and 98% for [11C]CLZ (Supplementary Figure S4).

Discussion

This study explored why the contrast (signal-to-background ratio) of the hM4Di receptor with [11C]DCZ has previously been found to be much higher than that of [11C]CLZ. The findings indicate that the higher signal-to-background ratio of [11C]DCZ compared to [11C]CLZ was primarily driven by its lower background uptake and that the contribution of improved selectivity was limited. The signal-to-background ratio (calculated as BP_{ND}') of [11C]DCZ was 1.8-fold higher than that of [11C]CLZ. In contrast, selectivity (calculated as the ratio of V_{s-on} to V_s) was comparable between [11C]DCZ and [11C]CLZ. The cause of the higher BP_{ND}' of [11C]DCZ was that its V_{ND}/f_P was about one-tenth that of [11C]CLZ, while V_{S-on}/f_P of [11C]DCZ was only about one-fifth that for [11C]CLZ. Based on calculated values of lipophilicity (clog$D$), the lipophilicity of [11C]DCZ was about six-fold less than that of [11C]CLZ. The lower lipophilicity of [11C]DCZ was the likely cause of its lower binding both to plasma proteins and to nonspecific sites in brain. The free fraction in plasma (f_P) of [11C]

DCZ was about four times that of [11C]CLZ, and the free fraction in brain (f_{ND}) of [11C]DCZ was almost 10 times that of [11C]CLZ. Taken together, the results thus suggest that the lower nonspecific binding in brain of [11C]DCZ was likely caused by its lower lipophilicity compared to that of [11C]CLZ.

In vitro binding studies to numerous receptors known to interact with [11C]CLZ have suggested that [11C]DCZ would have much less off-target binding than [11C]CLZ.[7] In fact, we found that the off-target binding (V_{S-off}/f_P mL·cm^{-3}) of [11C]DCZ (32) was one-sixth of that of [11C]CLZ (192) (Table 1). We do not know the source of this off-target binding, but it might be an endogenous muscarinic acetylcholine receptor. However, when measured as a percentage of all displaceable specific binding, the selectivity for on-target binding was similar for both radioligands, about 85%.

Effects of lipophilicity and affinity

Given the multiple components of radioligand uptake, it appears that most differences between the two radioligands can be explained by their relative affinity and lipophilicity. First, the in vitro inhibition constant (K_i) of [11C]DCZ (4.2 nM) was five-fold higher than that of [11C]CLZ (0.9 nM). Affinity also played a role in the amount of off-target binding of both radioligands.[7] The amount of both off-target and on-target binding of [11C]CLZ was five- to six-fold higher than that of [11C]DCZ, which reflects a similar increased affinity of DCZ compared to CLZ for both the transfected and endogenous receptor. Related to this parallel increase in affinity, the percentage of on-target binding of both radioligands was similar, about 85%. Second, the lipophilicity (clog$D$) of [11C]DCZ (2.59) was six-fold

lower than that of [^{11}C]CLZ (3.39), and lower lipophilicity is generally associated with lower nonspecific binding. The V_{ND} of [^{11}C]DCZ (5.8 mL $\cdot$ cm^{-3}) was three-fold lower than that of [^{11}C]CLZ (17.0 mL $\cdot$ cm^{-3}). Third, the f_{ND} of [^{11}C]DCZ (3.79%) was 11-fold higher than that of [^{11}C]CLZ (0.35%). These values were calculated from the formula $V_{ND} = f_P / f_{ND}$[14] and from our measured values of V_{ND} and f_P for each radioligand. f_{ND} tends to mirror f_P, as both reflect low affinity (non-displaceable) adsorption of radioligand to lipids and proteins in both tissues. Consistent with this notion, both the f_P and f_{ND} of [^{11}C]DCZ were higher than those of [^{11}C]CLZ (Supplementary Table S4).

Reference tissue models

All prior DREADD studies that employ PET have used reference tissue models to measure the density of the transfected receptor.[7,9] Using arterial blood sampling and compartmental model as the "gold standard", all reference tissue models were found to underestimate BP_{ND} (calculated without separating on-target and off-target displaceable binding) of the DREADD-injected region. The reference tissue models also underestimated BP_{ND} for all other brain regions. This underestimation occurred because the model assumes that the reference region (in our case, the cerebellum) contains no specific/displaceable binding. Reference tissue models may mis-estimate binding potential when one or more assumptions of the models are violated.[28] However, in the present study, any disruption of the blood-brain barrier at the time of viral injection is likely to have resolved by the time of the first PET scan (55 days later), suggesting that blood-brain barrier leak is unlikely to be a factor in interpreting the binding signal. Furthermore, although reference tissue models do not accurately measure the transfected receptor, they still provide a linear measure of receptor density if the reference region is unchanged between scans or between subjects, which is often the case. Such a region with specific/displaceable binding is called a "pseudo-reference region" and has been validated even for clinical studies.[29] Thus, we expect that [^{11}C]DCZ will continue to provide useful information regarding localization and comparative quantitation for hM$_4$Di DREADD.

Limitations

Three limitations bear mention. The first and potentially most significant limitation is that the study was conducted in a single animal. However, in the field of DREADD research in non-human primates, studies frequently report results drawn from only one or two animals. Second, on-target binding was operationally defined as the difference between the injection site and its contralateral region – i.e., right amygdala minus left amygdala. The underlying assumption was that the contralateral amygdala had no transfected receptors and that off-target binding was the same in both regions. Tracer studies confirm that no known homotopic amygdala projections exist in rhesus monkeys.[30,31] In addition, injection of the DREADD may have changed the density of off-target receptors. Nevertheless, our results indicate that off-target binding was a small percentage (15%–16%) of total displaceable binding.

Third, within the field of PET radioligand development, a 1.8-fold increase of BP_{ND}' is considered substantial, but its impact on quantitation is unclear. The impact may be estimated by comparing radioligands to another target: translocator protein 18 kDa (TSPO), a putative marker of neuroinflammation. (R)-[^{11}C]PK11195 was the prototypical radioligand for imaging TSPO, but the second-generation radioligand [^{11}C]PBR28 showed much greater sensitivity for detecting inflammation in neurological[32] and psychiatric disorders.[33] The BP_{ND} of [^{11}C]PBR28 (1.2) was 1.5-fold higher than that of (R)-[^{11}C]PK11195 (0.8),[34] suggesting that the 1.8-fold increased signal-to-background ratio of [^{11}C]DCZ compared to [^{11}C]CLZ may usefully improve sensitivity. For example, the improved sensitivity of DCZ might permit detection of regions to which the injection site projects.[7]

The results of these investigations have reinforced two important principles for the interpretation of images and the development of improved radioligands. First, the initial impression of a radioligand that provides higher contrast than another is that the specific binding is higher. In fact, contrast is a ratio, which was measured in this study as the ratio of specific to nondisplaceable uptake BP_{ND}'. As we have shown, higher contrast may be associated with both lower specific and lower nondisplaceable uptake; the net effect depends on the value of the ratio itself. A second principle applicable to groups that develop radioligands is the subtle interaction that exists between affinity (which is proportional to specific binding) and lipophilicity (which has complex effects on both affinity and nonspecific binding). In this case, development of an improved radioligand would be helped by additional structure-activity data on the effect of lipophilicity on affinity and nonspecific binding.

Conclusion

The signal-to-background ratio of [^{11}C]DCZ was greater than that of [^{11}C]CLZ primarily because of lower nonspecific binding of [^{11}C]DCZ. Both

radioligands had similar selectivity, that is, high-affinity displaceable binding to DREADDs relative to endogenous receptor(s). Using a plasma input function and a two-tissue compartmental model as the gold standard, reference models underestimated true values of the signal-to-background ratio. Nevertheless, the use of a pseudo-reference region should provide useful information on the localization and comparative quantitation of the transfected receptor. Taken together, the results confirm that $[^{11}C]DCZ$ is far superior to $[^{11}C]$CLZ to image the hM_4Di DREADD. Thus, $[^{11}C]DCZ$ should continue to be a valuable adjunct for behavioral and translational experiments.

Declaration of conflicting interests

The author(s) declared the following potential conflicts of interest with respect to the research, authorship, and/or publication of this article: YN and TM are named as inventors on a patent application (PCT/JP2019/024834; status: patent pending) claiming subject matter related to the results described in this paper. The remaining authors have no conflict of interest to disclose, financial or otherwise.

Authors' contributions

XY: conducted the literature search; conducted laboratory work; collected the data; conducted the statistical analysis; drafted the manuscript; revised the manuscript; approved the final version of the manuscript.
ST: conducted laboratory work; collected the data; revised the manuscript; approved the final version of the manuscript.
RMD: conducted the literature search; conducted laboratory work; revised the manuscript; approved the final version of the manuscript.
J-SL: conducted laboratory work; collected the data; assisted with statistical design, analysis, and interpretation; revised the manuscript; approved the final version of the manuscript.

PZ-F: helped interpret the statistical analysis; revised the manuscript; approved the final version of the manuscript
CLM: conducted laboratory work; revised the manuscript; approved the final version of the manuscript.
LSM: conducted laboratory work; revised the manuscript; approved the final version of the manuscript.
RLG: conducted laboratory work; revised the manuscript; approved the final version of the manuscript.
SS: conducted laboratory work; collected the data; revised the manuscript; approved the final version of the manuscript.
WL: conducted laboratory work; revised the manuscript; approved the final version of the manuscript.
YN: helped interpret the statistical analysis; revised the manuscript; approved the final version of the manuscript.
TM: conceptualized and designed the study; helped interpret the statistical analysis; revised the manuscript; approved the final version of the manuscript.
SSZ: conducted laboratory work; helped interpret the statistical analysis; revised the manuscript; approved the final version of the manuscript.
RBI: conceptualized and designed the study; assisted in the statistical design, analysis, and interpretation; revised the manuscript for critical intellectual content; provided research supervision; approved the final version of the manuscript.
VWP: conceptualized and designed the study; revised the manuscript; approved the final version of the manuscript.
BJR: conceptualized and designed the study; revised the manuscript; approved the final version of the manuscript.
MAGE: conceptualized and designed the study; conducted laboratory experiments; revised the manuscript; approved the final version of the manuscript.

ORCID iDs

Rachel M Dick (ID) https://orcid.org/0000-0003-4495-8811
Takafumi Minamimoto (ID) https://orcid.org/0000-0003-4305-0174
Barry J Richmond (ID) https://orcid.org/0000-0002-8234-1540
Mark AG Eldridge (ID) https://orcid.org/0000-0003-4292-6832

Supplemental material

Supplemental material for this article is available online.

References

1. Armbruster B and Roth B. Creation of designer biogenic amine receptors via directed molecular evolution. *Neuropsychopharmacology* 2005; 30: S265.
2. Armbruster BN, Li X, Pausch MH, et al. Evolving the lock to fit the key to create a family of G protein-coupled receptors potently activated by an inert ligand. *Proc Natl Acad Sci U S A* 2007; 104: 5163–5168.
3. Eldridge MA, Lerchner W, Saunders RC, et al. Chemogenetic disconnection of monkey orbitofrontal and rhinal cortex reversibly disrupts reward value. *Nat Neurosci* 2016; 19: 37–39.
4. Ferguson SM, Eskenazi D, Ishikawa M, et al. Transient neuronal inhibition reveals opposing roles of indirect and direct pathways in sensitization. *Nat Neurosci* 2011; 14: 22–24.

5. Alexander GM, Rogan SC, Abbas AI, et al. Remote control of neuronal activity in transgenic mice expressing evolved G protein-coupled receptors. *Neuron* 2009; 63: 27–39.

6. Becnel J, Johnson O, Majeed ZR, et al. DREADDs in drosophila: a pharmacogenetic approach for controlling behavior, neuronal signaling, and physiology in the fly. *Cell Rep* 2013; 4: 1049–1059.

7. Nagai Y, Miyakawa N, Takuwa H, et al. Deschloroclozapine, a potent and selective chemogenetic actuator enables rapid neuronal and behavioral modulations in mice and monkeys. *Nat Neurosci* 2020; 23: 1157–1167.

8. Ji B, Kaneko H, Minamimoto T, et al. Multimodal imaging for DREADD-Expressing neurons in living brain and their application to implantation of iPSC-Derived neural progenitors. *J Neurosci* 2016; 36: 11544–11558.

9. Bonaventura J, Eldridge MAG, Hu F, et al. High-potency ligands for DREADD imaging and activation in rodents and monkeys. *Nat Commun* 2019; 10: 4627.

10. Nagai Y, Kikuchi E, Lerchner W, et al. PET imaging-guided chemogenetic silencing reveals a critical role of primate rostromedial caudate in reward evaluation. *Nat Commun* 2016; 7: 13605.

11. Gomez JL, Bonaventura J, Lesniak W, Mathews WB, et al. Chemogenetics revealed: DREADD occupancy and activation via converted clozapine. *Science* 2017; 357: 503–507.

12. Manvich DF, Webster KA, Foster SL, et al. The DREADD agonist clozapine N-oxide (CNO) is reverse-metabolized to clozapine and produces clozapine-like interoceptive stimulus effects in rats and mice. *Sci Rep* 2018; 8: 3840.

13. Raper J, Morrison RD, Daniels JS, et al. Metabolism and distribution of clozapine-N-oxide: Implications for nonhuman primate chemogenetics. *ACS Chem Neurosci* 2017; 8: 1570–1576.

14. Innis RB, Cunningham VJ, Delforge J, et al. Consensus nomenclature for in vivo imaging of reversibly binding radioligands. *J Cereb Blood Flow Metab* 2007; 27: 1533–1539.

15. Jendryka M, Palchaudhuri M, Ursu D, et al. Pharmacokinetic and pharmacodynamic actions of clozapine-N-oxide, clozapine, and compound 21 in DREADD-based chemogenetics in mice. *Sci Rep* 2019; 9: 4522.

16. Synthia a. compact radiochemistry system for automated production of radiopharmaceuticals. In: *TRIUMF: Proceedings of the VIth Workshop on Targetry and Target Chemistry*, Vancouver, British Columbia, 17–19 August 1995.

17. Lu S, Hong J, Itoh T, et al. [carbonyl-C]benzyl acetate: automated radiosynthesis via Pd-mediated [C]carbon monoxide chemistry and PET measurement of brain uptake in monkey. *J Labell Comp Radiopharm* 2010; 53: 548–551.

18. Larsen P, Ulin J, Dahlstrøm K, et al. Synthesis of [11C] iodomethane by iodination of [11C]methane. *Appl Radiat Isotopes* 1997; 48: 153–157.

19. Holschbach M and Schüller M. An on-line method for the preparation of n.c.a. [11CH3] trifluoromethanesulfonic acid methyl ester. *Appl Radiat Isotopes* 1993; 44: 897–898.

20. Fredericks JM, Dash KE, Jaskot EM, et al. Methods for mechanical delivery of viral vectors into rhesus monkey brain. *J Neurosci Methods* 2020; 339: 108730.

21. Zhang W, Ramamoorthy Y, Kilicarslan T, et al. Inhibition of cytochromes P450 by antifungal imidazole derivatives. *Drug Metab Dispos* 2002; 30: 314–318.

22. Gandelman MS, Baldwin RM, Zoghbi SS, et al. Evaluation of ultrafiltration for the free-fraction determination of single photon emission computed tomography (SPECT) radiotracers: beta-CIT, IBF, and iomazenil. *J Pharm Sci* 1994; 83: 1014–1019.

23. Ichise M, Toyama H, Innis RB, et al. Strategies to improve neuroreceptor parameter estimation by linear regression analysis. *J Cereb Blood Flow Metab* 2002; 22: 1271–1281.

24. Akaike H. A new look at the statistical model identification. *IEEE Trans Automat Contr* 1974; 19: 716–723.

25. Golla SSV, Adriaanse SM, Yaqub M, et al. Model selection criteria for dynamic brain PET studies. *EJNMMI Phys* 2017; 4: 30.

26. Zoghbi SS, Shetty HU, Ichise M, Fujita M, et al. PET imaging of the dopamine transporter with ^{18}F-FECNT: a polar radiometabolite confounds brain radioligand measurements. *J Nucl Med* 2006; 47: 520–527.

27. Weber DA, Eckerman KF, Dillman LT, et al. *MIRD: radionuclide data and decay schemes*. New York: Society of Nuclear Medicine, 1989.

28. Salinas CA, Searle GE and Gunn RN. The simplified reference tissue model: model assumption violations and their impact on binding potential. *J Cereb Blood Flow Metab* 2015; 35: 304–311.

29. Lyoo CH, Ikawa M, Liow JS, et al. Cerebellum can serve as a pseudo-reference region in Alzheimer disease to detect neuroinflammation measured with PET radioligand binding to translocator protein. *J Nucl Med* 2015; 56: 701–706.

30. Aggleton JP, Burton MJ and Passingham RE. Cortical and subcortical afferents to the amygdala of the rhesus monkey (Macaca mulatta). *Brain Res* 1980; 190: 347–368.

31. Demeter S, Rosene DL and Van Hoesen GW. Fields of origin and pathways of the interhemispheric commissures in the temporal lobe of macaques. *J Comp Neurol* 1990; 302: 29–53.

32. Kreisl WC, Kim M-J, Coughlin J, et al. PET imaging of neuroinflammation in neurological disorders. *Lancet Neurol* 2020; 19: 940–950.

33. Meyer JH, Cervenka S, Kim M-J, et al. Neuroinflammation in psychiatric disorders: PET imaging and promising new targets. *Lancet Psychiatry* 2020; 7: 1064–1074.

34. Fujita M, Kobayashi M, Ikawa M, et al. Comparison of four 11C-labeled PET ligands to quantify translocator protein 18 kDa (TSPO) in human brain: (R)-PK11195, PBR28, DPA-713, and ER176-based on recent publications that measured specific-to-non-displaceable ratios. *EJNMMI Res* 2017; 7: 84.